Th A12

Low Salinity Waterflooding for Enhanced Oil Recovery - Stochastic Model Calibration and Uncertainty Quantification

M. Spagnuolo* (Eni S.p.A. Upstream and Technical Services), C. Callegaro (Eni S.p.A. Upstream and Technical Services), A. Guadagnini (Politecnico di Milano) & R. Sabatino (Eni S.p.A. Upstream and Technical Services)

SUMMARY

We focus on key aspects related to the quantification of the uncertainty associated with modeling of Enhanced Oil Recovery (EOR) through Low Salinity (LS) water injection in a reservoir. Low salinity waterflooding is an emerging EOR technique in which the salinity of the injected water is controlled to improve oil recovery, as opposed to conventional waterflooding where brine is usually used. Several mechanisms have been proposed to underpin the processes leading to additional oil mobility, but none of them has been conclusively identified as the key driving cause. Literature results suggest that LS water causes an alteration of the wettability of the porous medium, leading to more favorable conditions for oil recovery. In this context, simulation models that represent the process using salinity-dependent relative permeabilities have been developed.
Here, we consider a tertiary coreflood experiment performed at Eni laboratory facilities through LS water injection, following sea water flooding. Oil and water relative permeability curves are parameterized through the Corey model. Model parameters and their uncertainties are estimated within a stochastic inverse modeling approach, upon relying on a classical reservoir simulator to simulate the measured oil recovery. The likelihood function is maximized through a joint use of the Latin hypercube sampling and the Metropolis Hastings algorithm, while the process model is coupled with a universal Kriging technique. The posterior sample of model parameters is then employed to quantify uncertainty propagation to a sector model of a selected North-East African sandstone reservoir. This enables us to quantify the impact of parameter uncertainty on the expected oil production resulting from a field scale application of the technique under study. The reservoir simulation reveals the potential of the LS water injection technique to improve the recovery in the considered field.

Introduction

Low Salinity (LS) waterflooding is an emerging EOR technique based on the premise that injecting water with controlled salinity in a reservoir leads to improved oil recovery. The approach exploits the beneficial effects of conventional waterflooding, and induces a wettability alteration towards water-wet conditions, which are most favorable to oil mobilization.

Interpretation and modeling of the observed wettability alteration process relies on a variety of physical and chemical mechanisms associated, with diverse effects in sandstone and/or carbonate reservoirs. The two most highly regarded interpretive models are respectively based on *(a)* the occurrence of Multicomponent Ion Exchange (MIE) (Lager *et al*., 2006; Lee *et al*., 2010; Seccombe *et al*., 2010), or *(b)* the effects of pH on the adsorption onto the clay surface of polar components of the crude oil (Austad *et al*., 2010; Austad, 2012). Other mechanisms proposed include the migration of fines (Tang and Morrow, 1999), and the alkaline-flooding behavior (McGuire *et al*., 2005). Pu *et al*. (2010) suggest the relevance of mineral dissolution, while Sandengen & Arntzen (2013) discuss the role of osmosis. Recent results based on visual inspection of experimental settings evidence that formation of water micro-dispersion within the oil phase might takes place (Emadi and Sohrabi, 2013). In this context, no conclusive results are available in the literature and it is recognized that *(a)* the documented wettability alteration is likely due to a combination of factors, and *(b)* proper modeling of the process would require the integration within a unique theoretical framework of the concepts underpinning the models (Rotondi *et al*., 2014).

The physical-chemical mechanisms underlying the LS effect on EOR have been primarily modeled by representing the wettability change through salinity-dependent relative permeabilities (KRs). The latter are considered to direct the (multiphase) flow of fluids in porous and fractured media at the continuum scale, typical of Darcy-flow and field-scale engineering applications. The most relevant modeling-related work is the one proposed by Jerauld *et al*. (2006). The main features of this study are the definition of two sets of KR curves, respectively related to high and low salinity conditions, and the way salt is treated, i.e., it is considered as an additional single-lumped component present in the aqueous phase. This method was applied, e.g., by Marcolini *et al*. (2009).

Here, a tertiary laboratory-scale coreflood experiment performed through LS water injection is illustrated and modeled (Spagnuolo, 2014). Relative permeability curves are expressed through the well-established Corey model (Corey, 1954). The latter is calibrated within a stochastic inverse modeling approach. The posterior sample of model parameters is then employed on a field sector model representing a North-East African sandstone reservoir. Forecast scenarios, which include the injection of LS water, are studied to *(a)* quantify the propagation to the expected field-scale oil production of the uncertainty associated with estimates of the Corey model parameters; and *(b)* assessing the ability of the LS technique to improve oil recovery in the field setting considered.

Field overview

A giant onshore North-East African field was selected by eni S.p.A. for chemical EOR evaluation study on the basis of preliminary considerations based on the documented high (under-saturated) oil in place, low oil recovery and the system petrophysical attributes. The field was discovered in 1954 and production started in 1955 as primary depletion. Water injection, with an unfavorable mobility ratio, has been gradually implemented since 1985. The field is currently under secondary recovery. The latter is managed through waterflooding and high water cut is observed in most of the wells. The field can be described as an anticline, 10 km long and 4 km wide. A depth map of the field is depicted in Figure 1.

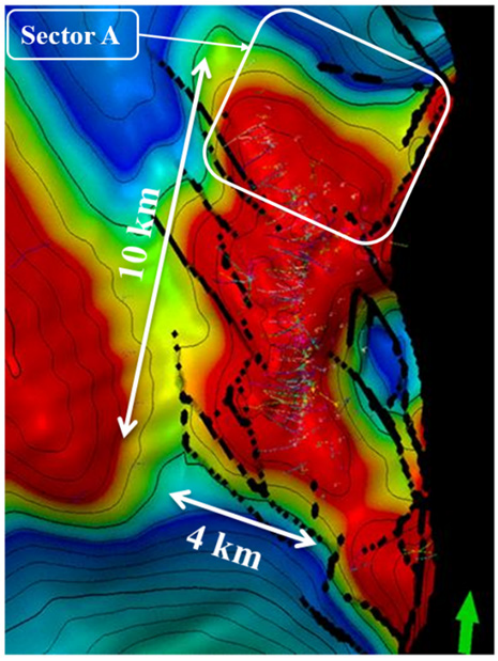

Figure 1 *Depth map for the selected North-East African field.*

The field is a multilayer system with interbedded shales and anhydrite intercalations ranging from Lower to Upper Miocene Age. Two major faulting systems roughly subdivide the structure into twelve sandstone reservoirs, which are in partial hydraulic communication. One of these, denoted as sector A, is a shallow system and is identified as a candidate zone for chemical EOR evaluation due to its relatively lower temperature distribution, good geological knowledge, high permeability and moderate heterogeneity, short distances between injectors and producers, documented beneficial effect of water injection, and relatively modest water cut. Relevant properties of sector A are listed in Table 1.

Table 1 *Relevant properties of sector A.*

Reservoir temperature [°C]	76
Oil density [kg/Sm^3]	933
Oil viscosity [cP]	8
Formation water salinity [ppm]	220,000
Average porosity [%]	19
Average permeability [mD]	400

Laboratory scale coreflooding test

Sector A of the considered field was designated by eni for EOR evaluation study. A new well was drilled in the area in 2010 and a core acquisition was performed. Plugs depicted in Figure 2 were selected for chemical EOR study on the basis of criteria including homogeneity of the porous medium, absence of fractures, mineralized material with limited clay content, and absence of cemented zones.

Figure 2 *Selected plugs from sector A.*

A coreflooding test was then performed to evaluate the additional oil recovery after tertiary LS water injection following High Salinity (HS) flooding. The geometrical and petrophysical plug characteristics are listed in Table 2. Fluid displacement was performed using two brines with different salinities: the HS water is seawater at salinity of 39,000 ppm Total Dissolved Solids (TDS), in line with actual water injection properties, while the LS water is characterized by a salinity of 3,000 ppm TDS. The HS water properties were measured, while the properties of LS water were estimated using salinity-dependent relationships. The dead oil, with density at standard conditions of 0.93 g/cm^3, was mixed with 25% of toluene, to match reservoir oil viscosity. Table 2 lists the properties of the fluids employed in the experiment. Fluid densities are given at standard conditions (15.5 °C and 1 atm), while fluid viscosities are evaluated at reservoir temperature and atmospheric pressure.

Table 2 *Plug characteristics and fluid properties.*

Plug characteristics		Fluid properties	
Length [cm]	7.85	Water (HS – LS) salinity [ppm]	39,000 – 3,000
Diameter [cm]	3.75	Water (HS – LS) density [g/cm^3]	1.05 – 0.98
Porosity [%]	22.54	Water (HS – LS) viscosity [cP]	0.54 – 0.36
Initial water saturation [%]	22	Oil density [g/cm^3]	0.915
Brine permeability [mD]	237	Oil viscosity [cP]	8

The experimental equipment used for the displacement test is sketched in Figure 3. The test was performed in a confined Hassler-type cell containing the core and placed inside an oven to reproduce reservoir temperature.

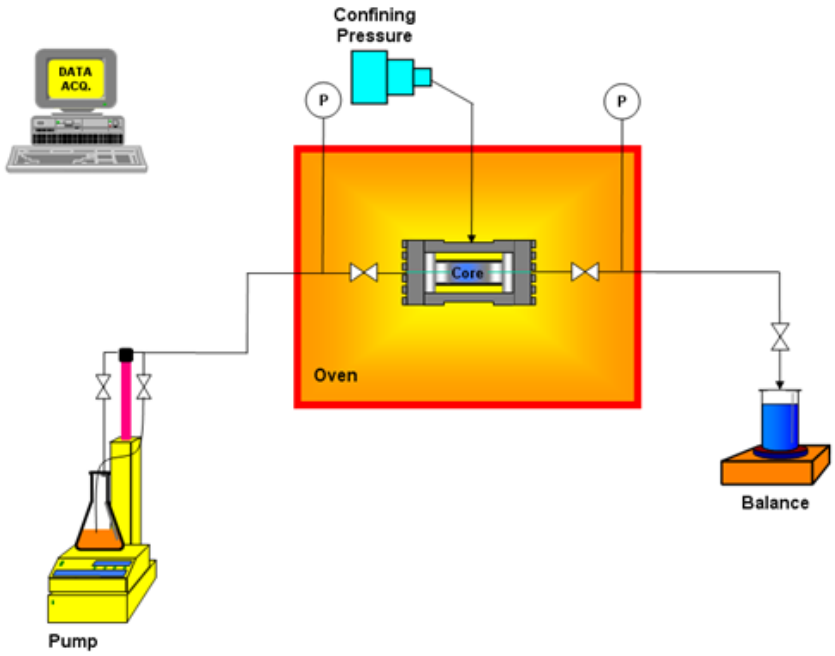

***Figure 3**. Sketch of the experimental set-up.*

The sample was cleaned with toluene and methanol at room temperature and dried before the test. It was then saturated with HS brine and aged to achieve equilibrium at ambient conditions. Flooding with oil at 76°C was performed, until irreducible water saturation was established, i.e., until no more water production was observed at the outlet of the plug. The flooding test was performed in two steps with constant injection rate of 1 cm^3/min. The first step was a flood with HS brine for a duration of 8 Pore Volumes (PV). The second step was a flood with LS brine for a duration of 72.5 PV. The fluid eluted from the core was weighted and sampled.

The experimental oil Recovery Factor (RF) is depicted in Figure 4, as a function of the volume of water injected. There is evidence of good oil recovery improvement as the RF increases from 44.2% (HS flood) to 59.3% (LS flood).

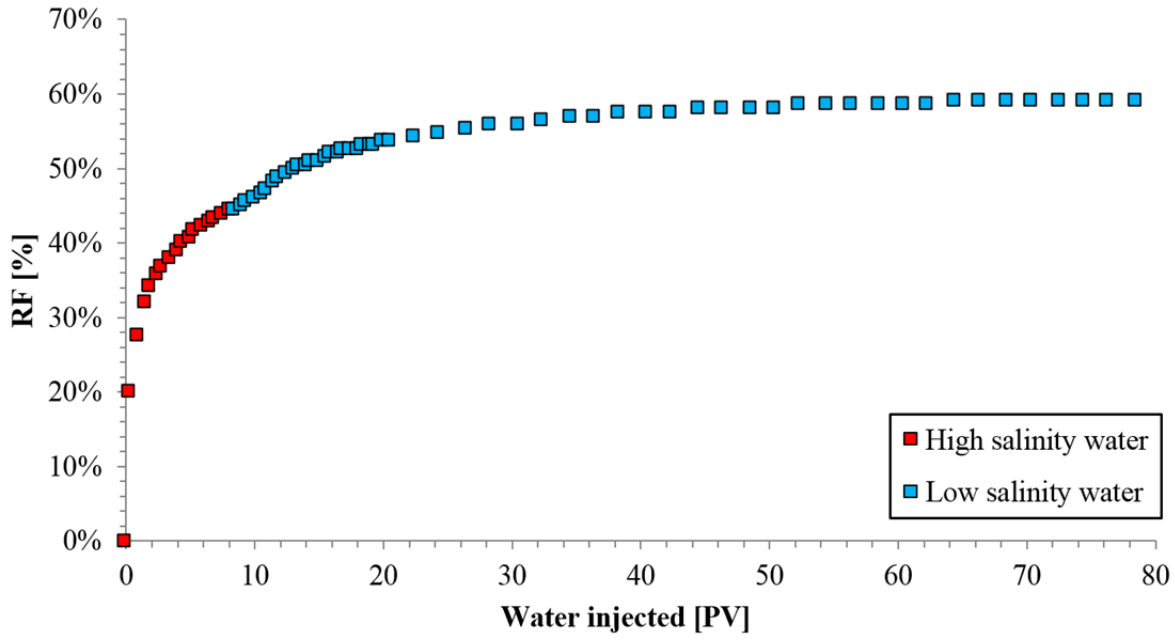

***Figure 4** Dependence of oil RF on volume of water injected.*

Coreflooding simulation

Simulation of the measured oil recovery is performed through the reservoir simulator ECLIPSE™ 100 (Schlumberger, 2012). The core sample is reproduced using a one-dimensional model. The domain is discretized through 100 grid blocks placed between two dummy wells, respectively serving as injector and producer. The simulation grid considered is depicted in Figure 5. The homogeneous petrophysical attributes and fluid properties listed in Table 2 are considered.

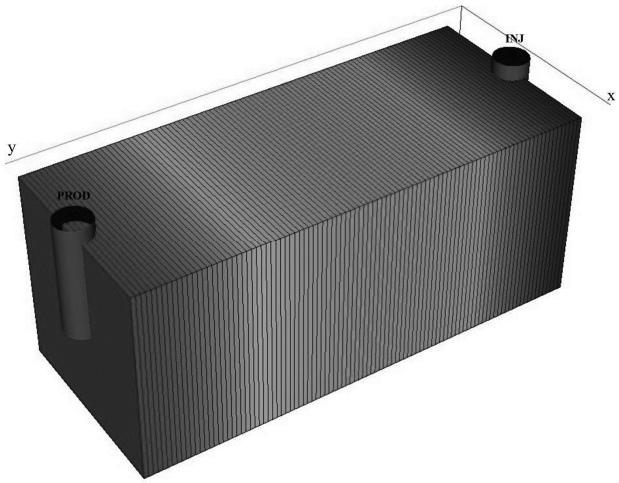

Figure 5 *Simulation grid.*

The system is assumed to be isothermal and composed of two fluid phases (aqueous and oil phase), and three mass components (water, oil, and salt), which are treated as single pseudo-components within the implemented Black Oil model. The two liquid components (water and oil) are assumed to be present only in their associated phases. Salt is contained only in the aqueous phase and subject to convection and dispersion processes. No chemical reactions or inter-phase mass exchange are considered. Adsorption of salt on the rock surface and the effects of capillary pressure are neglected.

The system is parameterized through the standard Corey model to express the two-phase KR curves:

$$k_{r,w} = k^{\circ}_{r,w}\left(\frac{S_w - S_{wir}}{1 - S_{wir} - S_{or}}\right)^{N_w} \tag{1}$$

$$k_{r,o} = k^{\circ}_{r,o}\left(\frac{1 - S_w - S_{or}}{1 - S_{wir} - S_{or}}\right)^{N_o} \tag{2}$$

Here, S_w is the water saturation, $k^{\circ}_{r,o}$ and $k^{\circ}_{r,w}$ respectively are the endpoint of the oil and water KR curves, N_o and N_w are the Corey exponents, and S_{wir} and S_{or} are the irreducible water saturation and the residual oil saturation, respectively.
The wettability alteration is represented with the LOWSALT option, implemented in ECLIPSE™. Two sets of saturation functions and two salinity thresholds ($c_{s,max}$=39,000 ppm and $c_{s,min}$=3,000 ppm) are defined. A linear interpolation of the values associated with HS and LS curves is employed to calculate local relative permeability, i.e.,

$$k_r = \omega k_r^{HS} + (1 - \omega)k_r^{LS} \tag{3}$$

The weight ω being dependent on local salt concentration. HS and LS curves are used when the calculated local salt concentration is outside the interval [$c_{s,min}$, $c_{s,max}$].

Stochastic model calibration

Estimate of model parameters and the associated uncertainty are assessed in a stochastic framework. Parameter estimation and model validation are performed within a stochastic inverse modeling framework, based on Maximum Likelihood Estimation (MLE) (Tarantola, 2005). Based on Eq. (1) and Eq. (2), the vector of model parameters is $\mathbf{m} = \left[k^{\circ}_{r,o}, k^{\circ}_{r,w}, N_o, N_w, S_{wir}, S_{or}\right]$. The observed data are the RF measurements, collected in vector $\mathbf{d_{obs}}$, while the simulated values of oil recovery, $\hat{\mathbf{d}}$, are linked to model parameters through the forward operator $\mathbf{g}(\cdot)$, i.e., $\hat{\mathbf{d}} = \mathbf{g}(\mathbf{m})$. The MLE of $\mathbf{m}$ is obtained by maximizing the likelihood function $\mathcal{L}(\mathbf{m})$. If, as commonly assumed, measurement errors are Gaussian distributed, $\mathcal{L}(\mathbf{m})$ can be expressed as:

$$\mathcal{L}(\mathbf{m}) = \frac{1}{\sqrt{(2\pi)^n \det(\mathbf{C_D})}} \exp\left[-\frac{1}{2}\left(\hat{\mathbf{d}} - \mathbf{d_{obs}}\right)^t \mathbf{C_D^{-1}}\left(\hat{\mathbf{d}} - \mathbf{d_{obs}}\right)\right] \tag{4}$$

$\mathbf{C_D}$ being the covariance matrix of measurement errors. The latter are considered to be uncorrelated and homoscedastic, i.e., associated with a constant variance σ_D^2, so that $\mathbf{C_D} = \sigma_D^2\mathbf{I}$, $\mathbf{I}$ being the identity matrix**.** In this setting, minimizing the Negative Log Likelihood (NLL) is tantamount to minimize the following Objective Function (OF):

$$OF = \frac{1}{n}\sum_{i=1}^{n} \frac{\left(d_{obs,i} - \hat{d}_i\right)^2}{\sigma_D^2} \tag{5}$$

n being the number of available measurements. It is worth observing that minimizing the OF corresponds to simulated values very close to the observed ones, i.e. models able to correctly reproduce the historical observations.

From an operational standpoint, MLE is implemented in the software MEPO, a reservoir optimization and risk analysis tool (SPT Group, 2012). The solution of the stochastic inverse problem is then obtained upon coupling *(a)* the Latin Hypercube (LH) sampling method (Helton and Davis, 2003), to generate the starting point in the parameter space according to prior probability distribution settings, and *(b)* the Metropolis Hastings Algorithm (MHA) (Tarantola, 2005), which allows exploring the model parameter space within the regions of significant likelihood of model parameters. Speed up of computational time is obtained by replacing the full system at each time step through a surrogate model that approximates the model input-output relation through a universal Kriging technique (Roustant *et al.*, 2012).

Estimation of the LS relative permeability curves starts with the definition of the prior distribution of model parameters, which is specified independent of the observed data. The Corey parameters are assumed to be uncorrelated and described by uniform distributions. Ranges of parameter variability are defined according to literature (Stiles, 2010). Starting parameter values are defined on the basis of a preliminary manual model calibration. Table 3 lists these settings.

Table 3 *Limits for the assumed prior uniform distribution and initial values of model parameters.*

Corey parameter	Lower limit	Upper limit	Start value
S_{wir}	0.20	0.24	0.22
N_w	2	6	3
$k^{\circ}_{r,w}$	0.1	0.5	0.3
$k^{\circ}_{r,o}$	0.8	1	1
N_o	2	6	3.25
S_{or}	0.15	0.4	0.28

The One-Variable-At-Time (OVAT) analysis is performed to assess the impact of the Corey parameters on the OF. The tornado chart depicted in Figure 6 displays the relative change on the OF due to the upper and lower limits defined in Table 3, compared to the base case (all parameters set to start value). These results reveal the relevant impact on the computed OF of S_{or} and N_o. It is noted that the computed OF is not sensitive to S_{wir}, due to the assigned narrow range of variability as it was experimentally measured, and $k^{\circ}_{r,o}$, which is physically of less importance as the displacement was performed in a tertiary way. The latter is then removed from the model parameter vector and is assigned a deterministic unit value.

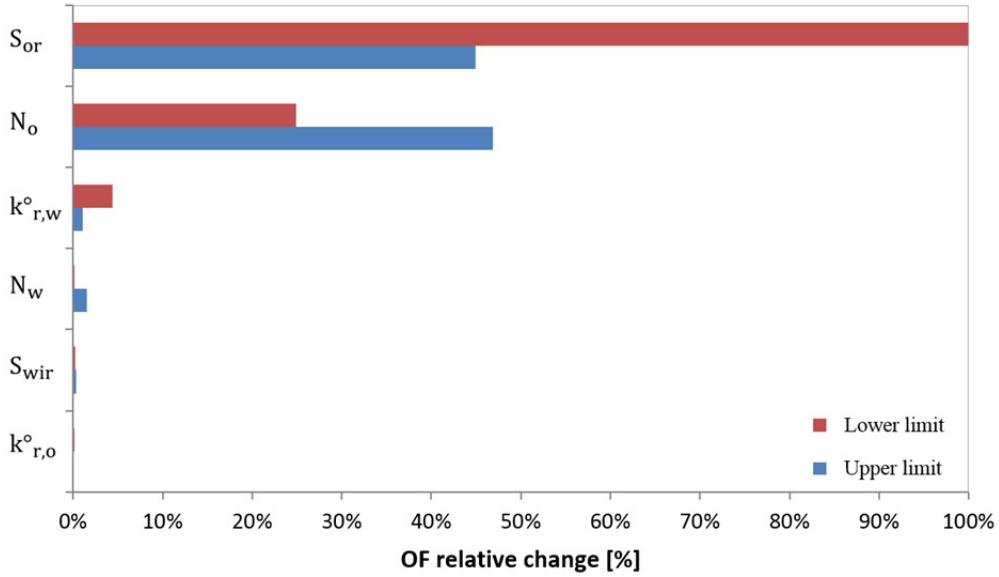

Figure 6 *Tornado chart from OVAT analysis. Upper and lower limits assumed for the definition of the parameter space are listed in Table 3.*

A number of 200 simulations are performed by sampling the model parameter space through the LH sampler. Surrogate models of the simulator are then built through a universal Kriging technique based on this initial collection of model parameter values, which is denoted as the current ensemble of model parameter. During the optimization loop, starting from 16 different set of model parameter values, the MHA generates chains of model parameter values according to a Gaussian distribution. The transition from one set of model parameters to another is accepted or rejected according to the Metropolis rule (Tarantola, 2005). The first 1,000 steps (burn-in length) in the model parameter space are excluded from the analysis to minimize dependency of results from the starting point. At each of the selected six iterations of the MHA, one sample of each chain is selected and the current ensemble of model parameter is updated.

Results of the stochastic model inversion are expressed through sampling from the posterior distribution of model parameters. Table 4 lists mean and standard deviation of 48 realizations of Corey parameters associated with the last three iterations (respectively denoted as IT4, IT5, IT6) of the MHA. Figure 7.a depicts the comparison between measured oil recovery and simulated values, Figure 7.b depicts the ensuing LS relative permeability curves. The shapes of these curves qualitatively reflect the expected water-wet conditions obtained, i.e., estimates of Corey parameters fall within the range of values characterizing water-wet settings (Stiles, 2010).

Table 4 *Sample mean and standard deviation of the set of estimated Corey parameters.*

Corey parameter	Mean	Standard deviation
S_{wir}	0.210	0.007
N_w	2.41	0.21
$k^{\circ}_{r,w}$	0.236	0.056
$k^{\circ}_{r,o}$	1	0
N_o	4.53	0.32
S_{or}	0.222	0.012

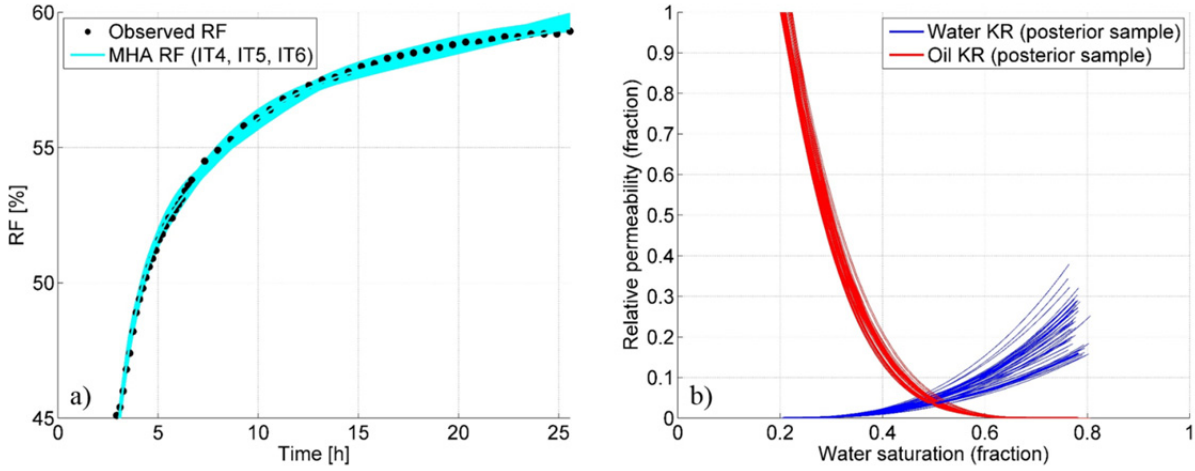

Figure 7 *MHA (IT4, IT5, IT6): (a) comparison between experiment and the set of 48 Monte Carlo inverse results; (b) associated LS KR curves.*

Analysis of the posterior distribution of Corey parameters reveals that these are cross-correlated. Figure 8 depicts the histograms of samples of selected oil and water Corey parameters, together with scatter plots to provide an appraisal of the degree of their correlation. The uniform prior probability density functions are also displayed for comparison. One can note that N_o and S_{or} are characterized by a high negative correlation.

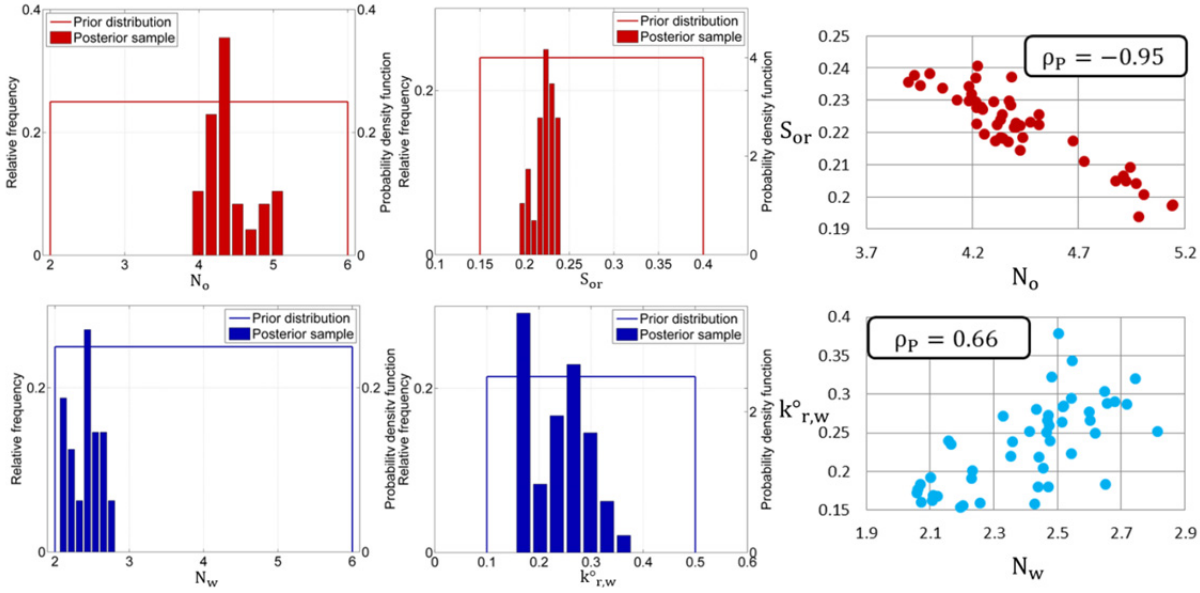

Figure 8 *Posterior sample of Corey parameters: histograms and scatter plots with Pearson correlation coefficient* ρ_P.

Reservoir sector simulation

The estimated uncertainty of model parameters is then propagated to the computed field-scale oil recovery. This is achieved by numerically simulating low salinity waterflooding in the sector model of the considered field.

This model includes 78 × 82 × 8 grid blocks (respectively along two normal horizontal axes and the vertical directions) with corresponding average cell dimensions of 50 × 50 × 2.5 m. Values of petrophysical and fluid properties are based on previous proprietary studies. In these works history matching was performed using the Ensemble Kalman Filter (EnKF) technique (Oliver *et al.*, 2008), resulting in multiple model realizations that honors pressure and rate history of the sector.

For the purpose of our comparative study, we simulate the wettability alteration in ECLIPSE™ using the LOWSALT option on a calibrated model scenario. High salinity KR curves were previously obtained from Special Core Analysis (SCAL) tests and are already implemented in the sector model. The water endpoint was considered an uncertain parameter during the history matching phase. A number of 30 EnKF realizations of high salinity KR curves are considered. Low salinity KRs are generated through the posterior sample of 48 realizations of Corey parameters found within the inverse modeling of the coreflood test described above. Figure 9 depicts the sets of HS and LS relative permeabilities implemented in the sector model.

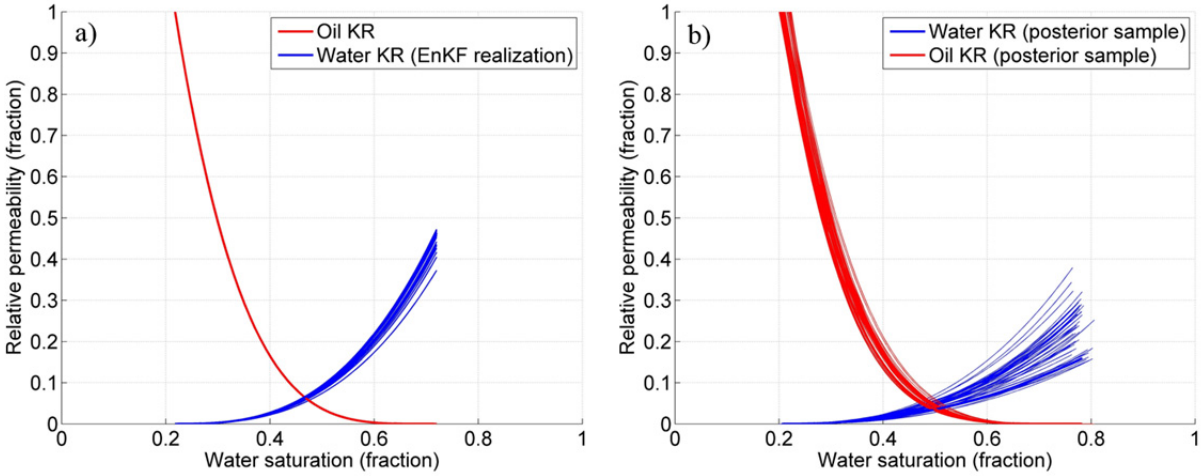

Figure 9 *(a) HS relative permeability curves; (b) LS relative permeability curves.*

The current deployment strategy in the area includes 12 oil producers and 3 peripheral seawater injectors, as showed in Figure 10. A new injector (NEW-INJ) is defined at a selected location, hereafter identified Region 2, which is considered as an optimal area to implement future chemical EOR techniques. The selected site, identified in red color in Figure 10, allows injecting through a dispersed pattern in a zone that is likely to reside within the drainage area of seven production wells, denoted as target wells in Figure 10. The new well injects LS water (salinity of 3,000 ppm TDS) at a constant rate (400 Sm^3/day) for a forecast duration of 10 years.

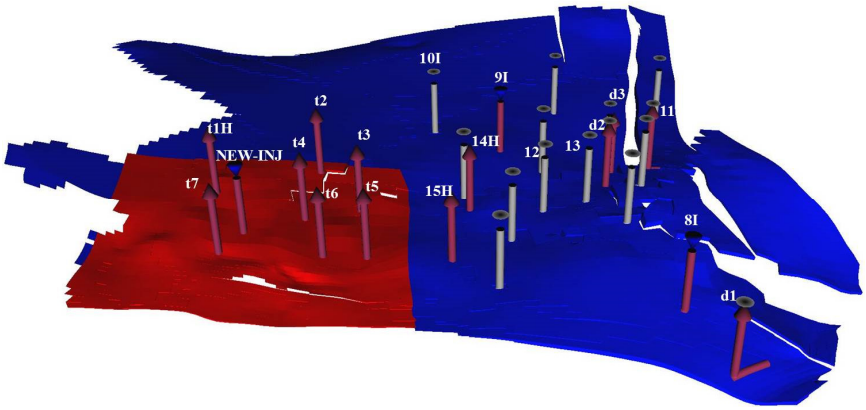

Figure 10 *Sector model with Region 2 coloured in red. NEW-INJ is the new injector considered. Producers in region 2 are identified by "t" (target) before their well number. "H" stands for horizontal, "I" for injector.*

Forecast scenarios are assessed in terms of incremental production as compared to a development strategy based on HS seawater (salinity 39,000 TDS) injection in the new well. Figure 11.a depicts the salt concentration at the final time for a selected setting. It is observed that only Region 2 is affected by a reduction of the salt concentration below the seawater salinity level. Figure 11.b depicts the collection of calculated oil production rate curves at well t4, the closest producer to the new injector, with the median of the values in bold line. Beneficial effects, as compared with the injection of HS seawater, are detected after the breakthrough of the main oil bank, which corresponds to the peak of oil production. The shut-in time for this well, i.e., the time at which the well is closed due to an exceedingly water production, is delayed by 1.5 years using LS water injection.

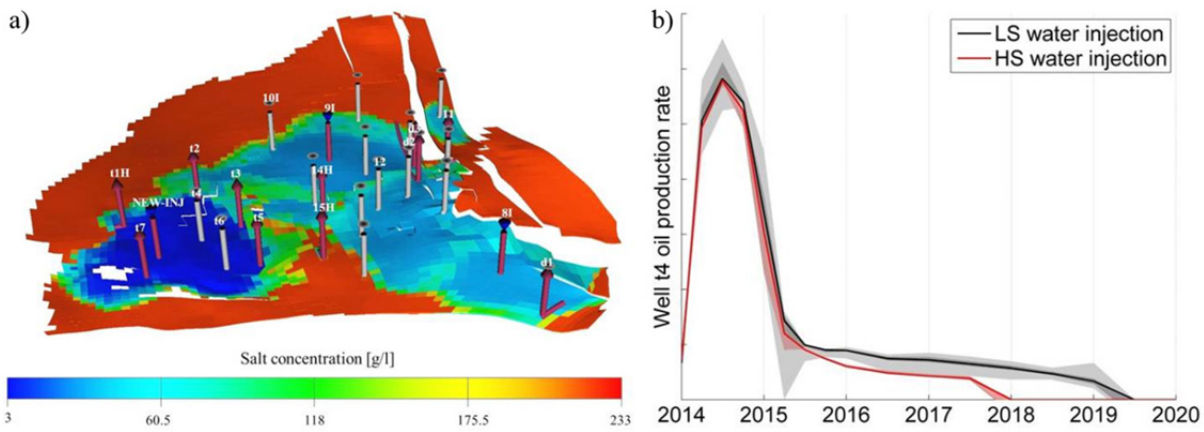

Figure 11 *Forecast scenarios: (a) salt concentration for a selected simulation; (b) collection of calculated oil production rate curves at well t4.*

Key conclusions can be obtained upon analyzing the RF of Region 2, i.e.,

$$\mathrm{RF} = \frac{\mathrm{ROPT}_2}{\mathrm{OOIP}_2} \tag{6}$$

representing the ratio of the Region 2 Oil Production Total (ROPT_2) and the Oil Originally In Place (OOIP_2). Figure 12.a depicts the oil RF curves, obtained for the LS and HS water injection scenarios. The reservoir response to LS waterflooding appears to be limited by the high salinity of the formation water (220,000 ppm TDS), which is suspected to be the main cause of reduction of the benefits associated with LS water to the improvement of oil recovery (Jerauld *et al.*, 2006). Figure 12.b depicts boxplots of $\mathrm{RF}_{\mathrm{LS}}$ and $\mathrm{RF}_{\mathrm{HS}}$ at July 2024. Sample means are 37.8% and 38.7%, respectively for HS

and LS water injection scenarios. It is concluded that there is evidence of enhanced oil recovery associated with LS water injection. Respectively denoting with μ_{LS} and μ_{HS} the average values of RF_{LS} and RF_{HS}, the width of the 95% confidence interval for $(\mu_{LS} - \mu_{HS})$ at July 2024 is (0.8 – 0.9)%. When compared against results associated with HS water injection, the additional oil production due to LS water injection is estimated to be 2.3%.

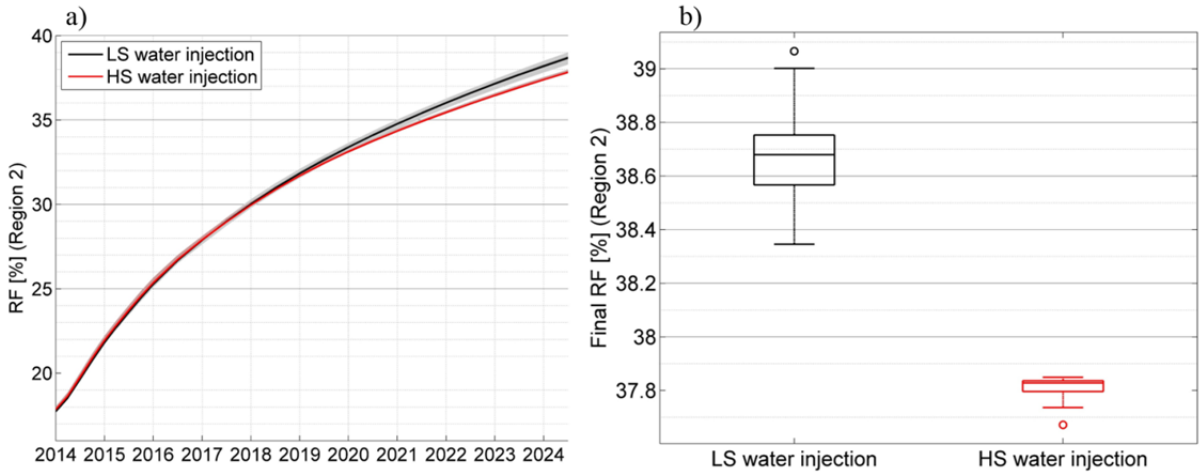

Figure 12 *Oil RF forecast in Region 2: (a) oil RF curves; (b) boxplots for ultimate oil recovery.*

Conclusions

We focus on the quantification of the uncertainty related to the prediction of Enhanced Oil Recovery (EOR) through Low Salinity (LS) waterflooding.

We perform stochastic inverse modeling of a tertiary coreflood experiment, conducted at eni laboratory with LS water. System parameterization is performed through the Corey model to express the salinity-dependent relative permeability (KR) curves. Model parameter estimation is based on laboratory-scale measured oil recovery. The likelihood function is maximized through a joint use of *(a)* the Latin Hypercube (LH) sampling method, and *(b)* the Metropolis Hastings Algorithm (MHA). Process modeling takes advantage of a surrogate model, which is built through a universal Kriging technique. A posterior sample of 48 low salinity KR curves has been obtained through a set of 200 LH realizations and 6 MHA iterations.

The estimated model parameters are then employed for reservoir simulation forecasts within a sandstone North-East African field sector model, selected for low salinity EOR evaluation. This enables us to estimate the propagation of the uncertainty of Corey parameters assessed at the core-scale to the computed oil recovery in the field-scale simulations. Forecast scenarios are simulated and compared with corresponding results from the adoption of HS water as an injection strategy. Our analysis suggests that LS water injection allows increasing the oil recovery in the monitoring area by approximately 0.8 - 0.9 %.

Further steps which are under scrutiny to assess actual LS waterflooding implementation include *(a)* implementation of pilot tests, in particular the Single Well Chemical Tracer Test (SWCTT), which was successfully executed with LS water in 2014 (Callegaro *et al.*, 2014); *(b)* feasibility studies of the required desalination facilities; and *(c)* additional uncertainty quantification studies. These studies, which could constitute further developments of the methodological framework illustrated in this work, may be related toward improved evaluation study. These can be performed, e.g., by fully coupling the effects of model parameter uncertainty (i.e. permeabilities and porosities) stemming from the history matching phase with those related to the stochastic inverse modeling approach. Model uncertainty could be analyzed through the application of model identification criteria (e.g., Bianchi Janetti *et al.*,

2012 and references therein) to evaluate the uncertainty arising from the use of alternative conceptual models to express KR curves.

Acknowledgements

The authors are grateful to the eni Upstream and Technical Services Division for permission to publish this work. The assistance and advice of Ernesto Della Rossa (eni S.p.A) is gratefully acknowledged.

Nomenclature

Abbreviations

EnKF	Ensemble Kalman Filter
EOR	Enhanced Oil Recovery
HS	High Salinity
KR	Relative permeability
LH	Latin Hypercube
LS	Low Salinity
MHA	Metropolis Hastings Algorithm
MIE	Multicomponent Ion Exchange
MLE	Maximum Likelihood Estimation
NLL	Negative Log Likelihood
OF	Objective Function
OOIP	Oil Originally In Place
OVAT	One-Variable-At-Time
PV	Pore Volume
RF	Recovery Factor
ROPT	Region Oil Production Total
TDS	Total Dissolved Solids

Symbols

c_s	Salt concentration
$\mathbf{C_D}$	Covariance matrix of measurement errors
$\hat{\mathbf{d}}$	Predicted data
$\mathbf{d_{obs}}$	Observed data
$\mathbf{g}(\cdot)$	Forward operator
$k_{r,o}$	Oil relative permeability
$k^{\circ}_{r,o}$	Oil endpoint relative permeability
$k_{r,w}$	Water relative permeability
$k^{\circ}_{r,w}$	Water endpoint relative permeability
$\mathcal{L}(\cdot)$	Likelihood function
$\mathbf{m}$	Model parameters
n	Number of data
N_o	Oil Corey exponent
N_w	Water Corey exponent
S_{or}	Residual oil saturation
S_w	Water saturation
S_{wir}	Irreducible water saturation
μ	Random variable mean
ρ_P	Pearson correlation coefficient
σ_D^2	Data variance
ω	Interpolation function

References

Austad, T. [2012] Water Based EOR in Carbonates and Sandstones: New Chemical Understanding of the EOR-Potential Using "Smart Water". Chapter in: Sheng, J. [2013] *Enhanced Oil Recovery Field Case Studies*. Elsevier, n.p.

Austad, T., RezaeiDoust, A. and Puntervold, T. [2010] Chemical Mechanism of Low Salinity Water Flooding in Sandstone Reservoirs. *SPE Improved Oil Recovery Symposium,* 24-28 April, Tulsa, Oklahoma, USA. SPE-129767-MS.

Bianchi Janetti, E., Dror, I., Guadagnini, A., Riva, M. and Berkowitz, B. [2012] Estimation of Single-Metal and Competitive Sorption Isotherms through Maximum Likelihood and Model Quality Criteria. *Soil Science Society of American Journal (SSSAJ),* **76**(4), 1229-1245.

Callegaro, C., Bartosek, M., Masserano, F., Nobili, M., Parasiliti Paracello, V., Pizzinelli, C. and Caschili, A. [2013] Opportunity of Enhanced Oil Recovery Low Salinity Water Injection: From Experimental Work to Simulation Study up to Field Proposal. *EAGE Annual Conference & Exhibition incorporating SPE Europec*, 10-13 June, London, UK. SPE-164827-MS.

Callegaro, C., Masserano, F., Bartosek, M., Buscaglia, R., Visintin, R., Hartvig, S.K. and Huseby, O.K. [2014] Single Well Chemical Tracer Tests to Assess Low Salinity Water and Surfactant EOR Processes in West Africa. *International Petroleum Technology Conference*, 10-12 December, Kuala Lumpur, Malaysia. IPTC-17951-MS.

Corey, A.T. [1954] The Interrelation Between Gas and Oil Relative Permeabilities. *Producers Monthly,* **19**(1), 38-41.

Emadi, A. and Sohrabi, M. [2013] Visual Investigation of Oil Recovery by Low Salinity Water Injection: Formation of Water Micro-Dispersions and Wettability Alteration. *SPE Annual Technical Conference and Exhibition,* 30 September-2 October, New Orleans, Louisiana, USA. SPE-166435-MS.

Helton, J.C. and Davis, F.J. [2003] Latin hypercube sampling and the propagation of uncertainty in analyses of complex systems. *Reliability Engineering & System Safety,* **81**(1), 23-69.

Jerauld, G.R., Webb, K.J. and Lin, C.Y. [2006] Modeling Low-Salinity Waterflooding. *SPE Annual Technical Conference and Exhibition,* 24-27 September, San Antonio, Texas, USA. SPE-102239-MS.

Lager, A., Webb, K.J., Black, C.J.J., Singleton, M. and Sorbie, K.S. [2006] Low Salinity Oil Recovery - An Experimental Investigation. *International Symposium of the Society of Core Analysts,* 12-16 September, Trondheim, Norway. SCA2006-36.

Lee, S.Y., Webb, K.J., Collins, I.R., Lager, A., Clarke, S.M., O'Sullivan, M., Routh, A.F. and Wang, X. [2010] Low Salinity Oil Recovery: Increasing Understanding of the Underlying Mechanisms. *SPE Improved Oil Recovery Symposium,* 24-28 April, Tulsa, Oklahoma, USA. SPE-129722-MS.

Marcolini, M., Masserano, F. and Battistelli, A. [2009] Preliminary Modeling of Rock Wettability Alteration During Low-Salinity Waterflooding Using TOUGH2-TMGAS. *TOUGH Symposium 2009*, 14-16 September, Lawrence Berkeley National Laboratory, Berkeley, California, USA.

McGuire, P.L., Chatham, J.R., Paskvan, F.K., Sommer, D.M. and Carini, F.H. [2005] Low Salinity Oil Recovery - An Exciting New EOR Opportunity for Alaska's Norh Slope. *SPE Western Regional Meeting,* 30 March-1 April, Irvine, California, USA. SPE-93903-MS.

Oliver, D.S., Reynolds, A.C. and Liu, N. [2008] *Inverse Theory for Petroleum Reservoir Characterization and History Matching.* Cambridge University Press, 2008.

Pu, H., Xie, X., Yin, P., Morrow, N.R. [2010] Low Salinity Waterflooding and Mineral Dissolution. *SPE Annual Technical Conference and Exhibition*, 19-22 September, Florence, Italy. SPE-134042-MS.

Rotondi, M., Binda, A., Draoui, M., Tsoumou, A. and Tealdi, L. [2011] Monitoring and Improving Water Injection Efficiency in a Structurally Complex Field. *SPE Annual Technical Conference and Exhibition*, 30 October-2 November, Denver, Colorado, USA. SPE-146817-MS.

Rotondi, M., Callegaro, C., Masserano, F. and Bartosek, M. [2014] Low Salinity Water Injection: eni's Experience. *Abu Dhabi International Petroleum Exhibition and Conference*, 10-13 November, Abu Dhabi, UAE. SPE-171794-MS.

Roustant, O., Ginsbourger, D. and Deville, Y. [2012] DiceKriging, DiceOptim: Two R Packages for the Analysis of Computer Experiments by Kriging-Based Metamodeling and Optimization. *Journal of Statistical Software,* **51**(1), 1-55.

Sandengen, K. and Arntzen, O.J. [2013] Osmosis During Low Salinity Water Flooding. *EAGE IOR 2013 – 17th European Symposium on Improved Oil Recovery,* 16-18 April, St. Petersburg, Russia.

Schlumberger [2012] ECLIPSE Version 2012.2 - Technical Description.

Seccombe, J., Lager, A., Jerauld, G., Jhaveri, B., Buikema, T., Bassler, S., Denis, J., Webb, K., Cockin, A., Fueg, E. and Paskvan, F. [2010] Demonstration of Low-Salinity EOR at Interwell Scale, Endicott Field, Alaska. *SPE Improved Oil Recovery Symposium,* 24-28 April 2010, Tulsa, Oklahoma, USA. SPE-129692-MS.

Spagnuolo, M. [2014] *Low Salinity Waterflooding for Enhanced Oil Recovery: Inverse Modeling and Uncertainty Quantification.* Master Thesis. Politecnico di Milano, Milano.

SPT Group [2012] MEPO 4.2 User Manual.

Stiles, J. [2010] Special Core Analysis (SCAL). *HOT Engineering*, eni in-house course.

Tang, G. and Morrow, N.R. [1999] Influence of brine composition and fines migration on crude oil/brine/rock interactions and oil recovery. *Journal of Petroleum Science & Engineering,* **24**(2-4), 99-111.

Tarantola, A. [2005] *Inverse Problem Theory and Methods for Model Parameter Estimation.* Society for Industrial and Applied Mathematics (SIAM), Philadelphia.